PERGAMON

International Journal of Solids and Structures 40 (2003) 3331–3345

INTERNATIONAL JOURNAL OF SOLIDS and STRUCTURES

www.elsevier.com/locate/ijsolstr

Analysis of multi-layered microelectronic packaging under uniformly distributed loading

Yujun Wen, Cemal Basaran *

UB Electronic Packaging Laboratory, Department of Civil, Structural and Environmental Engineering, University at Buffalo, SUNY, 212 Ketter Hall, North Campus, Buffalo, NY 14260-4300, USA

Received 19 August 2002; received in revised form 13 January 2003

Abstract

An accurate estimate of interfacial stresses in multi-layered microelectronic packaging is very important for design and prediction of delamination-related failures. An analytical model for stress analysis of multi-layered stacks, which is based on an extension of Valisetty's model (Bending of Beams, Plates and Laminates: Refined Theories and Comparative Studies, Ph.D. thesis, Georgia Institute of Technology, Atlanta, March 1983), is proposed in this paper. This analytical approach considers each layer as a beam-type plate with orthotropic material properties. A new miniature material testing unit is developed. High sensitive Moiré interferometry was used to measure the strain field in the bi-material interfaces. The test data is in good agreement with the proposed analytical solution. The problem is also analyzed by a finite element analysis. Comparison of all three results indicates that the analytical procedure is far superior to finite element analysis for this problem.

Keywords: Microelectronic packaging; Interfacial stress; Multi-layered structure; Interfacial delamination; Moiré interferometry

1. Introduction

Many researchers studied the failure mechanisms in multi-layered microelectronic packaging. An extensive literature survey on the subject is presented by Basaran and Zhao (2001) below some of these papers are highlighted. Delamination-related failures are the main problems at interfaces near the free edges. An accurate estimate of interfacial stresses is needed for predicting the delamination failures. Many investigators gave the numerical solutions for layered free edge problems. Pipes and Pagano (1970) analyzed this problem with finite difference method. Wang and Crossman (1977) gave the finite element solution for the same problem. Wang and Dixon (1978) extended Galerkin procedures. In addition, various studies (Lo et al., 1977a,b; Levinson, 1980; Bert, 1984; Cho et al., 1987) of higher-order plate theory have been reported since Reissner (1975) introduced higher-order forms for longitudinal and transverse displacements.

* Corresponding author. Tel.: +1-716-645-2429; fax: +1-716-645-3733.
E-mail address: cjb@eng.buffalo.edu (C. Basaran).

0020-7683/03/$ - see front matter © 2003 Elsevier Science Ltd. All rights reserved.
doi:10.1016/S0020-7683(03)00092-1

Cho et al. (1987) used higher-order theory in each layer separately which resulted in good agreement with Pagano's exact elastic-theory solution for a composite laminate in cylindrical bending (Pagano, 1969).

Hayashi (1967) presented the first analytical model that focused on the computation of interfacial shear stress. Hayashi model was based on the implicit assumption that the in-plane stresses within a given layer are independent of the thickness coordinate. Chen et al. (1982) took a very different approach, which satisfied the boundary conditions at the free edges of a laminated beam. The analysis was based on two-dimensional elasticity theory and the variational theorem of complementary energy (Washizu, 1968) under the assumption of linear distribution of longitudinal normal strain through the thickness of each layer. A similar approach was applied by Williams (1985) and showed good agreement with Chen et al. (1982). Bogy (1968, 1970), Hein and Erdogan (1971) and Yin (1991) discussed stress singularities at the interfaces near the free edges. Such stress singularities cannot be directly determined by the standard elastic finite element analysis alone. Asymptotic analysis is needed around the junction point to determine the stresses in the near-tip stress field (Lee and Jasiuk, 1991; Shih and Asaro, 1988, 1989). Shih and Asaro (1988, 1989) studied elastic–plastic analysis of cracks on bi-material interfaces, where they showed mesh dependence of finite element analysis and necessity of asymptotic analysis. In real life, such stress singularity ($1/r$) cannot exist, physically. Once the stress level reaches the yield strength of the material, ductile materials yield and brittle material cracks and stress is re-distributed to neighboring points. Basaran and Zhao (2001) have shown that when damage mechanics based elastic–viscoplastic material models are used in finite element method stress singularity ceases to be a significant issue.

Pagano (1974, 1978) firstly employed the ply mechanics technique to analyze composite laminates. Each layer (or a sublaminate) is treated as a homogeneous body in equilibrium independent of the laminate. The refined engineering theories (Valisetty and Rehfield, 1983; Valisetty, 1983; Rehfield and Valisetty, 1984) for homogeneous plates and laminated plates provided another alternative for the layer or sublaminate models.

This paper is an extension of the model proposed by Valisetty (1983) with emphasis on the stress behavior along the interfaces due to uniformly distributed loading. The primary common drawback of the proposed models is that none of them have been verified by test data on an actual microelectronic package. The model proposed in this paper has been verified in the lab by using a high sensitivity Moiré interferometry. Testing was conducted on an actual microelectronic Ball Grid Array package.

2. Formulation of analytical model

Consider an N-layer laminated beam-type plate as shown in Fig. 1. A summary of the basic equations for generic ply is given as follows. The overall equations of equilibrium and the constitutive equations for the beam-type plate theory will constitute a set of $8N$ equations in terms of a number of variables ($2N$ displacements, N rotations, $3N$ force resultants, and $2N$ moment resultants). This set is supplemented by an additional $2(N-1)$ equations, which are necessary for the simultaneous solution of $2(N-1)$ interfacial stresses, if the displacement continuity is enforced at $(N-1)$ laminar interfaces. Among this set of equations the force-resultant and moment-resultant variables can be eliminated with the aid of constitutive equations; these eliminations leave a set of $(5N-2)$ coupled differential equations to be solved for $2N$ displacement variables, N rotations, and $2(N-1)$ interfacial stresses.

Neglecting body forces, body moments and all derivatives with respect to X_1, we can write the following force and moment equilibrium equations for each layer using the stresses in kth layer:

$$N^k_{2,2} + n^k_2 = 0 \tag{1}$$

$$M^k_{2,2} + c_k m^k_2 - Q^k_2 = 0 \tag{2}$$

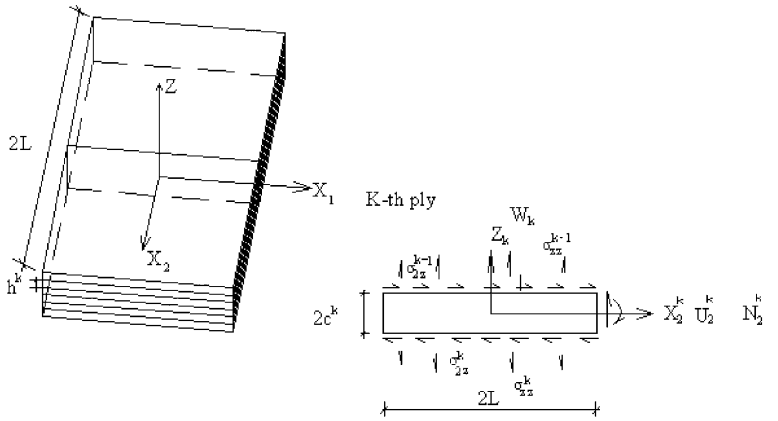

Fig. 1. Generic laminated beam-type plate.

$$Q^k_{2,2} + q^k = 0 \tag{3}$$

where comma identifies differentiation w.r.t. the axis number after the comma. Superscript k identifies kth ply. The difference in interfacial stresses between layers k and $k-1$ yield the stress imposed on each layer, which can be given by,

$$\begin{aligned} n^k_2 &= \sigma^{k-1}_{2z}(x_2, c_k) - \sigma^k_{2z}(x_2, -c_k) \\ m^k_2 &= \sigma^{k-1}_{2z}(x_2, c_k) + \sigma^k_{2z}(x_2, -c_k) \\ q^k &= \sigma^{k-1}_{zz}(x_2, c_k) - \sigma^k_{zz}(x_2, -c_k) \end{aligned} \tag{4a, b, c}$$

where N_2, M_2, Q_2 are, respectively, the force, moment, and shear resultants per unit width of the plate, associated with the X_2 coordinate direction, and n_2, m_2 and q are the load intensities for each layer related to interfacial stresses. $N_{2,2}$, $M_{2,2}$, $Q_{2,2}$ are, respectively, the derivatives of N_2, M_2, Q_2 with respect to X_2. The semi-thickness of the kth ply is c^k. Superscript k, which identifies the generic ply, will be dropped in the subsequent equations for convenience.

Most microelectronic packaging have orthotropic material properties. Moreover the loading is usually in the form of a thermal gradient or uniformly distributed loading. Hence we modify Valisetty beam-type plate model to introduce uniformly distributed loading and thermal gradient. In constitutive relations we also modify the coefficients $\overline{C}_{ij}$ and $\overline{C}_i$ to introduce the orthotropic material properties. As a result we obtain the following constitutive relations:

$$\begin{aligned} \frac{N_i}{h} &= -\overline{C}_{ij}\Delta T\,\alpha_j + \overline{C}_{i2}U_{2,2} + K_{ni}cn_{2,2} + K_{pi}p; \quad i,j = 1,2 \\ \frac{M_i}{\overline{I}} &= -\overline{C}_{i2}W_{,22} + K_{mi}m_{2,2} + K_{qi}q/c \\ \Phi_2 + W_{,2} &= \frac{c^2}{2\overline{I}}S_{44}\left(Q_2 - \frac{1}{3}cm_2\right) \end{aligned} \tag{5a, b, c}$$

where

$$K_{mi} = (3\overline{C}_{i2}S_{3j}\overline{C}_{j2}/\overline{C}_{22} - 2\overline{C}_{i2}S_{44} + 2\overline{C}_i)/20; \quad i,j = 1 \text{ and } 2$$
$$K_{qi} = (3\overline{C}_{i2}S_{3j}\overline{C}_{j2}/\overline{C}_{22} - 12\overline{C}_{i2}S_{44} + 12\overline{C}_i)/20$$
$$K_{ni} = (\overline{C}_{i2}S_{3j}\overline{C}_{j2}/\overline{C}_{22} + \overline{C}_{i2}S_{44} + 2\overline{C}_i)/12$$
$$K_{pi} = \overline{C}_i/2$$
$$p = \sigma_{zz}(x_2, c) + \sigma_{zz}(x_2, -c)$$
$$h = 2c, \quad \overline{I} = 2c^3/3$$

$$\overline{C}_{11} = C_{11} - \frac{C_{13}C_{31}}{C_{33}}, \quad \overline{C}_{12} = C_{12} - \frac{C_{13}C_{32}}{C_{33}}$$
$$\overline{C}_{21} = C_{21} - \frac{C_{23}C_{31}}{C_{33}}, \quad \overline{C}_{22} = C_{22} - \frac{C_{23}C_{32}}{C_{33}} \tag{6}$$
$$\overline{C}_1 = \frac{C_{13}}{C_{33}}, \quad \overline{C}_2 = \frac{C_{23}}{C_{33}}$$

C_{ij} is the stiffness coefficients of orthotropic materials, α_j, coefficient of thermal expansion of kth layer in direction j, ΔT, thermal gradient, U, W are the displacement components in the x_2- and z-direction, respectively, at $z = 0$ surface and Φ_2 is the rotation of a normal to the reference surface ($z = 0$).

Solution of the differential equations for the classical plate theory with beam-like behavior assumptions yield the following stress and displacement distribution equations:

$$\sigma_i = \frac{1}{h}N_i + \frac{1}{2h}K_i n_{2,2}(z^2 - c^2/3) + \frac{z}{\overline{I}}M_i + \frac{1}{6\overline{I}}K_i(cm_{2,2} + q)(z^3 - 3c^2z/5); \quad i,j = 1,2$$
$$\sigma_{2z} = \frac{z}{h}n_2 + \frac{c}{6\overline{I}}m_2(3z^2 - c^2) - \frac{1}{2\overline{I}}Q_2(z^2 - c^2) \tag{7a, b, c}$$
$$\sigma_{zz} = \frac{1}{2}p - \frac{1}{2h}n_{2,2}(z^2 - c^2) + \frac{z}{h}q - \frac{1}{6\overline{I}}(cm_{2,2} + q)(z^3 - c^2z)$$

where

$$K_i = \overline{C}_{i2}S_{3j}\overline{C}_{2j}/\overline{C}_{22} + \overline{C}_{i2}S_{44} - \overline{C}_i; \quad i,j = 1,2 \tag{8}$$

σ_1 is the normal stress in the x_1-direction in any layer, σ_2, normal stress in the x_2-direction, in any layer, σ_{2z}, shear stress in the x_2–z plane, σ_{zz}, transverse normal stress in the thickness coordinate z-direction, peeling stress.

$$w = W + S_{3j}\left(N_j\frac{z}{h} + M_j\frac{z^2}{2\overline{I}}\right) + S_{3j}K_j\frac{1}{6h}n_{2,2}(z^3 - c^2z) + S_{3j}K_j\frac{cm_{2,2} + q}{6\overline{I}}(z^4/4 - 3c^2z^2/10)$$
$$+ S_{33}\left(\frac{z}{2}p + \frac{z^2}{2h}q\right) - S_{33}\frac{1}{6h}n_{2,2}(z^3 - 3c^2z) - S_{33}\frac{cm_{2,2} + q}{6\overline{I}}(z^4/4 - c^2z^2/2) + z\Delta T\alpha_z \quad j = 1,2$$
$$u_2 = U_2 - zW_{,2} - S_{3j}\left(N_j\frac{z^2}{2h} + M_j\frac{z^3}{6\overline{I}}\right)_{,2} - S_{3j}K_j\left\{\frac{n_{2,22}}{6h}(z^4/4 - c^2z^2/2) + \frac{cm_{2,22} + q_{,2}}{6\overline{I}}(z^5/20 - c^2z^3/10)\right\}$$
$$- S_{33}\left\{\frac{z^2}{4}p_{,2} - \frac{1}{6h}n_{2,22}(z^4/4 - 3c^2z^2/2) + \frac{z^3}{6h}q_{,2} - \frac{cm_{2,22} + q_{,2}}{6\overline{I}}(z^5/20 - c^2z^3/6)\right\}$$
$$+ S_{44}\left\{\frac{z^2}{2h}n_2 + \frac{1}{6\overline{I}}cm_2(z^3 - c^2z) - \frac{1}{6\overline{I}}Q_2(z^3 - 3c^2z)\right\} \tag{9a, b}$$

where w, u_2 are the displacement components in the z and x_2 coordinate directions respectively.

3. Verification of the model

In order to verify the analytical model, an actual microelectronic Ball Grid Array (BGA) type microprocessor package is used. Fig. 2 shows the picture of the actual package used in this study. The first layer is BT substrate, the second layer is eutectic Pb/Sn solder, and the third layer is silicon die. The width of the specimen is 7.04 mm. High sensitivity Moiré interferometry was utilized to measure the strain field in the package. The geometry of the idealized model is shown in Fig. 3. The specimen was subjected to uniformly distributed load. In order to keep the behavior in elastic region the applied load is very small 0.0388 N/mm. Table 1 shows the orthotropic material properties as well as the dimensions and uniformly distributed load level used in this study. Material properties were obtained using a nanoindenter and by testing the actual package itself.

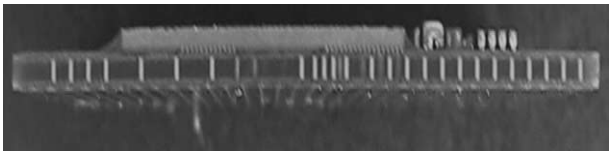

Fig. 2. Cross section of the actual BGA package.

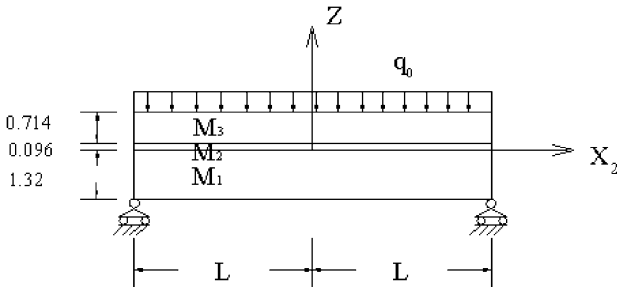

Fig. 3. Idealized model and loading of the specimen.

Table 1
Material properties, dimensions and loading information

	M_1 (BT)	M_2 (Pb/Sn solder)	M_3 (silicon)
E_1 (GPa)	17.5	24.3	112
E_2 (GPa)	10.4	24.3	148
E_3 (GPa)	4.7	24.3	168
G_{12} (GPa)	3.54	9.2	46.2
G_{13} (GPa)	9.04	9.2	33.2
G_{23} (GPa)	1.58	9.2	51.7
ν_{12}	0.32	0.32	0.28
ν_{13}	0.32	0.32	0.28
ν_{23}	0.32	0.32	0.28
h (mm)	1.32	0.096	0.714
$2L \times b$ (mm)		20.5×7.04	
q_0 (N/mm)		0.0388	

Assuming perfect displacement compatibility at the interfaces, the continuity requirement of displacements yields the following equations:

$$\begin{aligned} u_2^1\left(x_2,\frac{h_1}{2}\right) &= u_2^2\left(x_2,-\frac{h_2}{2}\right) \\ u_2^2\left(x_2,\frac{h_2}{2}\right) &= u_2^3\left(x_2,-\frac{h_3}{2}\right) \\ w^1\left(x_2,\frac{h_1}{2}\right) &= w^2\left(x_2,-\frac{h_2}{2}\right) \\ w^2\left(x_2,\frac{h_2}{2}\right) &= w^3\left(x_2,-\frac{h_3}{2}\right) \end{aligned} \tag{10a, b, c, d}$$

There are 10 unknowns and 10 equations. They are W^1, W^2, W^3, U_2^1, U_2^2, U_2^3, σ_{zz}^1, σ_{zz}^2, σ_{2z}^1, and σ_{2z}^2 where σ_{zz}^1 is the peeling stress at interface 1, σ_{zz}^2, peeling stress at interface 2, σ_{2z}^1, shear stress at interface 1, σ_{2z}^2 is the shear stress at interface 2.

We introduce the following boundary conditions for this problem:

at $x_2 = 0$:

$$\begin{aligned} &U_2^1 = 0, \quad \Phi_2^1 = 0, \quad Q_2^1 = 0 \\ &U_2^2 = 0, \quad \Phi_2^2 = 0, \quad Q_2^2 = 0 \\ &U_2^3 = 0, \quad \Phi_2^3 = 0, \quad Q_2^3 = 0 \end{aligned} \tag{11a}$$

at $x_2 = L$:

$$\begin{aligned} &N_2^1 = 0, \quad M_2^1 = 0, \quad W^1 = 0 \\ &N_2^2 = 0, \quad M_2^2 = 0, \quad W^2 = 0 \\ &N_2^3 = 0, \quad M_2^3 = 0, \quad W^3 = 0 \end{aligned} \tag{11b}$$

Using a hyperbolic solution we can obtain the following analytical solutions for this problem ($\xi = x_2/L$):

$$\begin{aligned} \sigma_{2z}^1 = {} & 0.244179\xi + 1.1039 \times 10^{-13}\xi^3 - 1.698 \times 10^{-24}\xi^4 + 1.3238 \times 10^{-24}\xi^5 \\ & - 7.77263 \times 10^{-11}\cosh(19.1422\xi)\sin(8.04406\xi) \\ & + 5.72243 \times 10^{-38}\cosh(80.1373\xi)\sin(47.1544\xi) \\ & + 1.58829 \times 10^{-92}\cosh(206.985\xi)\sin(145.569\xi) \\ & - 2.5206 \times 10^{-6}\sinh(9.89979\xi) + 5.8532 \times 10^{-27}\sinh(58.1214\xi) \\ \sigma_{2z}^2 = {} & 0.256381\xi - 2.08316 \times 10^{-13}\xi^3 + 1.91455 \times 10^{-24}\xi^4 - 1.49263 \times 10^{-24}\xi^5 \\ & - 7.6981 \times 10^{-11}\cosh(19.1422\xi)\sin(8.04406\xi) \\ & - 1.02923 \times 10^{-36}\cosh(80.1373\xi)\sin(47.1544\xi) \\ & - 3.07981 \times 10^{-92}\cosh(206.985\xi)\sin(145.569\xi) \\ & - 1.93177 \times 10^{-6}\sinh(9.89979\xi) + 8.15591 \times 10^{-27}\sinh(58.1214\xi) \\ & - 2.47146 \times 10^{-12}\cos(8.04406\xi)\sinh(19.1422\xi) \\ & + 6.38423 \times 10^{-37}\cos(47.1544\xi)\sinh(80.1373\xi) \\ & + 3.1741 \times 10^{-94}\cos(145.569\xi)\sinh(206.985\xi) \end{aligned}$$

$$
\begin{aligned}
\sigma_{zz}^{1} = & -0.0192352 - 2.21652\times10^{-14}\xi^{2} - 5.54753\times10^{-20}\xi^{4} + 4.32498\times10^{-20}\xi^{5} \\
& + 2.26043\times10^{-6}\cosh(9.89979\xi) - 7.66168\times10^{-27}\cosh(58.1214\xi) \\
& - 5.40925\times10^{-11}\cos(8.04406\xi)\cosh(19.1422\xi) \\
& - 7.08402\times10^{-38}\cos(47.1544\xi)\cosh(80.1373\xi) \\
& - 8.1104\times10^{-92}\cos(145.569\xi)\cosh(206.985\xi) \\
& - 3.16073\times10^{-11}\sin(8.04406\xi)\sinh(19.1422\xi) \\
& - 1.23006\times10^{-37}\sin(47.1544\xi)\sinh(80.1373\xi) \\
& - 1.11601\times10^{-91}\sin(145.569\xi)\sinh(206.985\xi) \\
\sigma_{zz}^{2} = & -0.0215826 - 1.55024\times10^{-14}\xi^{2} + 6.76039\times10^{-20}\xi^{4} - 5.27055\times10^{-20}\xi^{5} \\
& + 2.46604\times10^{-6}\cosh(9.89979\xi) - 1.16335\times10^{-26}\cosh(58.1214\xi) \\
& - 4.79321\times10^{-11}\cos(8.04406\xi)\cosh(19.1422\xi) \\
& - 3.74523\times10^{-38}\cos(47.1544\xi)\cosh(80.1373\xi) \\
& - 3.71061\times10^{-93}\cos(145.569\xi)\cosh(206.985\xi) \\
& - 1.7806\times10^{-11}\sin(8.04406\xi)\sinh(19.1422\xi) \\
& + 4.47561\times10^{-37}\sin(47.1544\xi)\sinh(80.1373\xi) \\
& + 5.56227\times10^{-94}\sin(145.569\xi)\sinh(206.985\xi) \\
W^{1} = & -0.00411616 + 0.0048809\xi^{2} - 0.000748132\xi^{4} - 0.0000101263\xi^{5} \\
& - 7.81453\times10^{-10}\cosh(9.89979\xi) + 6.70124\times10^{-32}\cosh(58.1214\xi) \\
& + 4.64708\times10^{-15}\cos(8.04406\xi)\cosh(19.1422\xi) \\
& - 2.82542\times10^{-43}\cos(47.1544\xi)\cosh(80.1373\xi) \\
& - 4.44478\times10^{-98}\cos(145.569\xi)\cosh(206.985\xi) \\
& + 7.75408\times10^{-15}\sin(8.04406\xi)\sinh(19.1422\xi) \\
& + 4.39039\times10^{-43}\sin(47.1544\xi)\sinh(80.1373\xi) \\
& + 6.62423\times10^{-98}\sin(145.569\xi)\sinh(206.985\xi) \\
W^{2} = & -0.00413873 + 0.00490336\xi^{2} - 0.000748132\xi^{4} - 0.0000101263\xi^{5} \\
& - 6.69307\times10^{-10}\cosh(9.89979\xi) + 4.17166\times10^{-32}\cosh(58.1214\xi) \\
& + 4.33801\times10^{-16}\cos(8.04406\xi)\cosh(19.1422\xi) \\
& - 6.90151\times10^{-43}\cos(47.1544\xi)\cosh(80.1373\xi) \\
& - 2.40261\times10^{-99}\cos(145.569\xi)\cosh(206.985\xi) \\
& + 2.67108\times10^{-17}\sin(8.04406\xi)\sinh(19.1422\xi) \\
& - 2.65463\times10^{-42}\sin(47.1544\xi)\sinh(80.1373\xi) \\
& - 2.55026\times10^{-97}\sin(145.569\xi)\sinh(206.985\xi)
\end{aligned}
$$

$$
\begin{aligned}
W^3 = & -0.0041398 + 0.00490446\xi^2 - 0.000748132\xi^4 - 0.0000101263\xi^5 \\
& - 6.36534 \times 10^{-10}\cosh(9.89979\xi) - 8.2022 \times 10^{-33}\cosh(58.1214\xi) \\
& + 2.05363 \times 10^{-16}\cos(8.04406\xi)\cosh(19.1422\xi) \\
& - 2.82143 \times 10^{-43}\cos(47.1544\xi)\cosh(80.1373\xi) \\
& - 1.44152 \times 10^{-99}\cos(145.569\xi)\cosh(206.985\xi) \\
& + 3.77458 \times 10^{-17}\sin(8.04406\xi)\sinh(19.1422\xi) \\
& + 2.64981 \times 10^{-43}\sin(47.1544\xi)\sinh(80.1373\xi) \\
& + 1.96037 \times 10^{-99}\sin(145.569\xi)\sinh(206.985\xi) \\
U_2^1 = & \ 0.000837783\xi - 0.000292504\xi^3 + 0.000208293\xi^4 - 0.00016239\xi^5 \\
& + 2.1838 \times 10^{-10}\sinh(9.89979\xi) - 1.97618 \times 10^{-31}\sinh(58.1214\xi) \\
& + 4.48702 \times 10^{-15}\cosh(19.1422\xi)\sin(8.04406\xi) \\
& - 1.76933 \times 10^{-42}\cosh(80.1373\xi)\sin(47.1544\xi) \\
& - 4.5257 \times 10^{-97}\cosh(206.985\xi)\sin(145.569\xi) \\
& - 4.37536 \times 10^{-16}\cos(8.04406\xi)\sinh(19.1422\xi) \\
& + 3.77441 \times 10^{-44}\cos(47.1544\xi)\sinh(80.1373\xi) \\
& + 3.95631 \times 10^{-99}\cos(145.569\xi)\sinh(206.985\xi) \\
U_2^2 = & \ 0.000250836\xi - 0.0000822119\xi^3 + 0.000208293\xi^4 - 0.00016239\xi^5 \\
& - 2.85709 \times 10^{-10}\sinh(9.89979\xi) + 8.57583 \times 10^{-34}\sinh(58.1214\xi) \\
& + 4.8129 \times 10^{-16}\cosh(19.1422\xi)\sin(8.04406\xi) \\
& + 1.89974 \times 10^{-43}\cosh(80.1373\xi)\sin(47.1544\xi) \\
& + 8.24727 \times 10^{-98}\cosh(206.985\xi)\sin(145.569\xi) \\
& + 5.34755 \times 10^{-16}\cos(8.04406\xi)\sinh(19.1422\xi) \\
& - 5.96538 \times 10^{-42}\cos(47.1544\xi)\sinh(80.1373\xi) \\
& - 2.60274 \times 10^{-98}\cos(145.569\xi)\sinh(206.985\xi) \\
U_2^3 = & -0.000133259\xi + 0.0000380824\xi^3 + 0.000208293\xi^4 - 0.00016239\xi^5 \\
& - 2.1825 \times 10^{-11}\sinh(9.89979\xi) + 9.83664 \times 10^{-33}\sinh(58.1214\xi) \\
& - 1.44349 \times 10^{-16}\cosh(19.1422\xi)\sin(8.04406\xi) \\
& - 7.06139 \times 10^{-43}\cosh(80.1373\xi)\sin(47.1544\xi) \\
& - 1.99438 \times 10^{-98}\cosh(206.985\xi)\sin(145.569\xi) \\
& + 1.3021 \times 10^{-16}\cos(8.04406\xi)\sinh(19.1422\xi) \\
& + 5.70578 \times 10^{-43}\cos(47.1544\xi)\sinh(80.1373\xi) \\
& + 7.70085 \times 10^{-100}\cos(145.569\xi)\sinh(206.985\xi) \qquad (12)
\end{aligned}
$$

Fig. 4. Experimental setup.

4. Experimental setup

Fig. 4 shows the experimental setup. A miniature material tester unit was developed and manufactured for this project. The testing unit uses DC-Mike Actuator M-235.5DG to apply the force. The actuator can be connected with a computer to control the displacement. The resolution for the actuator is 0.016 μm, and the maximum travel range is 50 mm. It can apply a maximum force of 120 N. There is a loadcell that is used to measure the applied force between the actuator and the specimen. The capacity for the loadcell ALD-SP-UTC-M-F-250 is 125 N. An aluminum block (thickness 9.7 mm) is placed between the specimen and the loadcell to obtain a uniformly distributed loading. We did have to try several different thickness blocks to obtain uniform loading. Moiré interferometry was very instrumental to see that there is no bending in the aluminum block and load is uniform. Special grease is applied between the block and actuator to prevent the application of lateral load component. Most important feature of this miniature material testing unit is that it fits very easily on an optical table to take real-time data with Moiré interferometry. Moreover it can be used for testing specimens too small for commercially available miniature material testers.

Moiré interferometry is an optical technique for determining in-plane displacements and strains, and features very high displacement sensitivity and spatial resolution. It uses two coherent beams of a laser to generate interferometric fringe pattern that carries the information of in-plane deformation of the object surface. A thin layer of epoxy is applied to the specimen surface to replicate an optical diffraction grating on the surface. The diffraction grating deforms with the specimen surface as the specimen is loaded, and the diffracted light records every detail of the deformed lines of the grating and hence records the deformation of specimen surface. The fringe pattern can be related to in-plane deformation as

$$\begin{aligned} U &= \frac{N_x}{f} \\ V &= \frac{N_y}{f} \end{aligned} \tag{13}$$

where U is the displacement in x-direction, V, the displacement in y-direction, N_x, the fringe order from U field, N_y, the fringe order from V field and f is the frequency of reference grating, 1200 lines/mm.

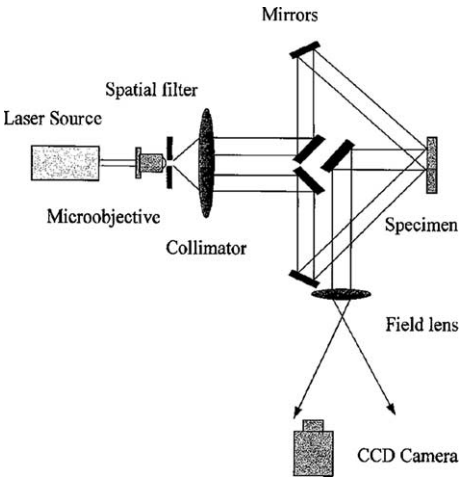

Fig. 5. Schematic illustration of two-beam Moiré interferometry.

The resolution of Moiré interferometry used in this work is 0.417 μm/fringe.

Fig. 5 shows the schematic illustration of two-beam Moiré interferometry to record the N_x and N_y fringe patterns that depict the U and V displacement fields. Once the displacements are available the total strains are computed by differentiation of the displacement distributions with respect to the two basic directions: horizontal (x) and vertical (y). The strains are given by

$$\begin{aligned}\varepsilon_x &= \frac{1}{f}\left[\frac{\partial N_x}{\partial x}\right]\\ \varepsilon_y &= \frac{1}{f}\left[\frac{\partial N_y}{\partial y}\right]\\ \gamma_{xy} &= \frac{\partial U}{\partial y}+\frac{\partial V}{\partial x}=\frac{1}{f}\left[\frac{\partial N_x}{\partial y}+\frac{\partial N_y}{\partial x}\right]\end{aligned} \tag{14}$$

Fig. 6(a) shows the initial U fringe field. Fig. 6(b)–(d) show the U fringe field for $P = 5.6$, 14 and 29.6 N, respectively. Initial V fringe field is shown in Fig. 7(a). Fig. 7(b)–(d) show the V fringe field for $P = 5.6$, 14 and 29.6 N, respectively. The P load value is the loadcell registered value. Due to aluminum block the package is subjected to a uniformly distributed load given by $q_0 = P/(2L \times b)$.

It should be pointed out that fringe fields shown in Figs. 6 and 7 are not perfectly symmetric. This is due to the fact that almost all microelectronic packages have initial manufacturing defects such as voids. Moiré interferometry easily picks up these defects as long as they are larger than 0.417 μm in any dimension.

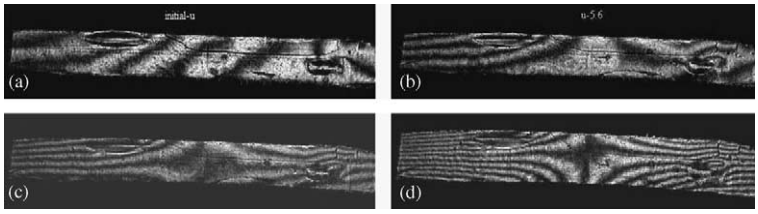

Fig. 6. (a) Initial U field. U field for (b) $P = 5.6$ N, (c) $P = 14$ N, and (d) $P = 29.6$ N.

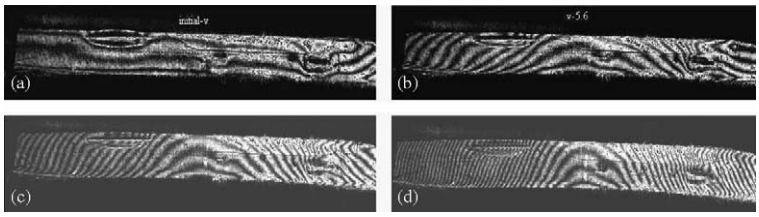

Fig. 7. (a) Initial V field. V field for (b) $P = 5.6$ N, (c) $P = 14$ N, and (d) $P = 29.6$ N.

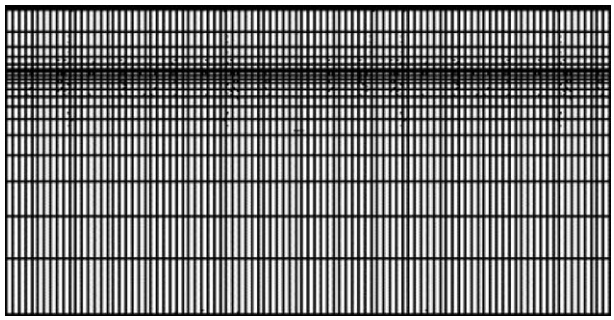

Fig. 8. Illustration of the FEA model for the three-layered problem.

5. Finite element analysis

The present example problem was also analyzed by a two-dimensional FEA using general-purpose finite element code ANSYS with quadrilateral elements under the plane strain condition in the x_2–z plane. Fig. 8 shows a mesh of elements for this problem. The total number of elements is 8400. This is a fine mesh and yields reasonable results according to an earlier study by Basaran and Zhao (2001).

6. Results and discussion

The deflection of the package is shown in Fig. 9 for FEA, test data and analytical solutions, respectively. Excellent agreement is shown with these three methods. Fig. 10 shows the axial normal stress distribution for BT layer along the longitudinal direction for FEA, test data and analytical solutions, respectively. The analytical solution is in very good agreement with FEA, but different from the test data by a difference of 22.4%.

Figs. 11 and 12 show the shear stress distribution along interfaces one and two for FEA, test data and analytical solutions, respectively. Figs. 13 and 14 show the distribution of peeling stress at interfaces one and two for FEA, test data and analytical solutions, respectively. Numeration of layers starts from the bottom.

The distribution of interfacial shear stresses and peeling stresses by the present theory gives good agreement with the results by the experiment. Both quantitative and qualitative values for the results are very close between the experiment and the analytical solutions. On the other hand even though FEA yields qualitatively close results, quantitative FEA results are far off from test data and analytical results. In Figs. 11 and 12 shear stresses monotonically increase and reach the maximum values at the free edge for the

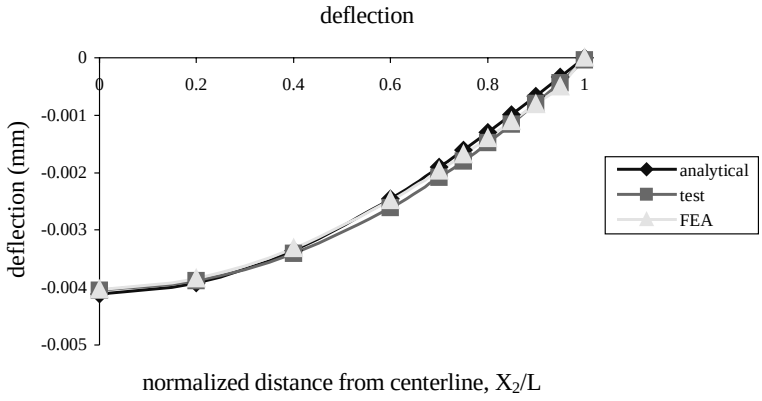

Fig. 9. Comparison of the deflection for FEA, test and analytical solution.

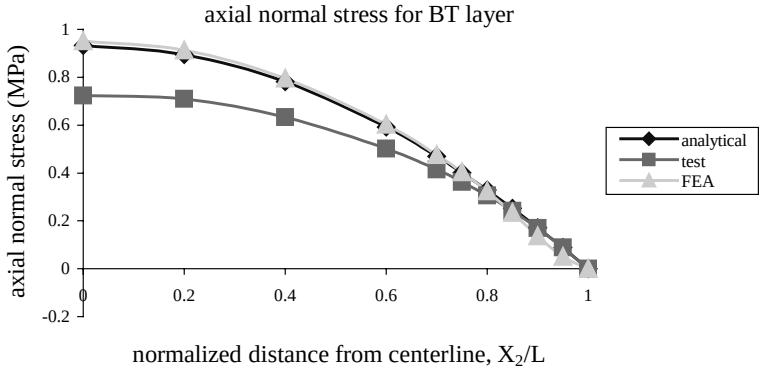

Fig. 10. Comparison of axial normal stress for BT layer for FEA, test and analytical solution.

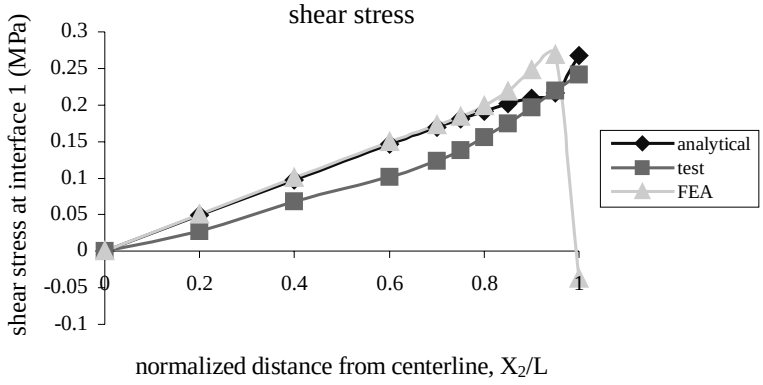

Fig. 11. Comparison of shear stress at interface 1 for FEA, test and analytical solution.

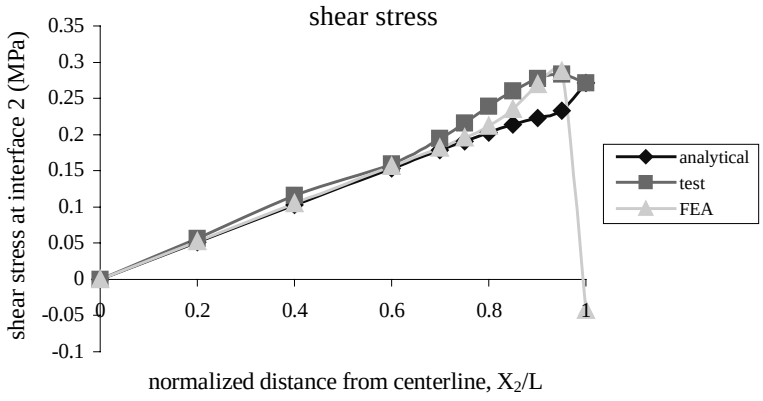

Fig. 12. Comparison of shear stress at interface 2 for FEA, test and analytical solution.

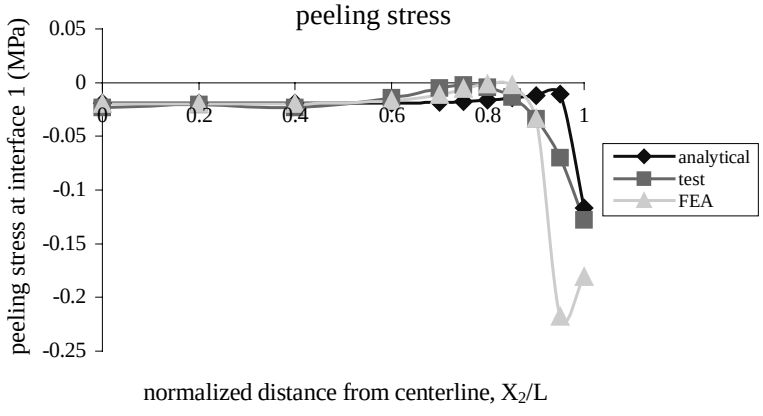

Fig. 13. Comparison of peeling stress at interface 1 for FEA, test and analytical solution.

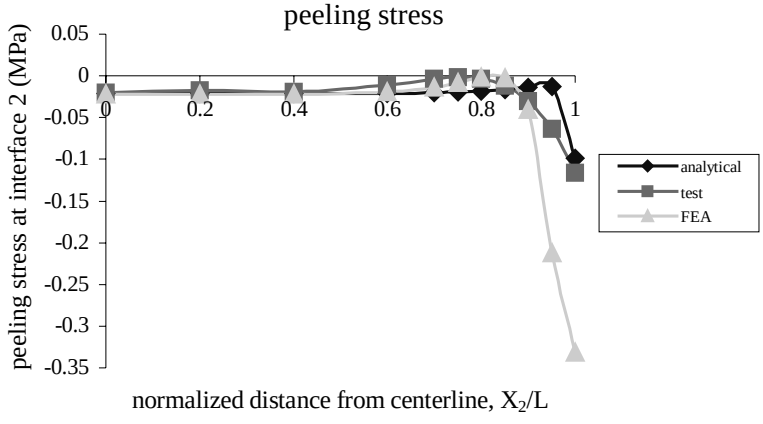

Fig. 14. Comparison of peeling stress at interface 2 for FEA, test and analytical solution.

analytical approach, but increase firstly then drop dramatically to get to a negative value at the free edge for FEA. In Fig. 13 the peeling stress monotonically decreases and reaches the minimum value at the edge for both analytical approach and experiment, but decreases firstly and then increase near the edge for FEA. In Fig. 14 the peeling stresses monotonically decrease and reach the minimum values at the free edge for the analytical approach, experiment and FEA. The minimum values for peeling stresses are very close between experiment results and analytical solutions, but quite different from FEA. Basaran and Zhao (2001) have shown that linear-elastic FEA suffers from mesh sensitivity for layered composite structures. Mesh sensitivity in layered bi-material structures is due to stress singularity near the free edge. To be able to use FEA for this problem a separate asymptotic analysis is required. On the other hand the proposed method does not suffer from the stress singularity at the edge. Experimental results obviously do not show stress singularity at 0.417 μm resolution. As has been shown by Basaran and Zhao (2001) in real life stress singularity is due to the solution of elasticity equation not a material response where stress reaches infinity. In reality as Moiré fringes show high stresses at the edge are redistributed to neighboring parts. The agreement between experiments and analytical procedure shows that the present analytical solution is reasonably accurate for estimating the interfacial stresses under uniformly distributed loading.

7. Conclusions

An analytical procedure based on classical plate theory for calculating interfacial shear and peeling stresses in layered structures under uniformly distributed loading and thermal gradient is presented. The model has been verified for uniformly distributed loading case. This method takes into account orthotropic material properties. The proposed method has been verified by high sensitivity Moiré interferometry. The analytical results are in good agreement with experiment results. Comparison of analytical, experimental and finite element analysis indicate that no matter how fine the finite element mesh is it cannot capture the actual physical behavior near the free edge even qualitatively. Hence the analytical procedure is much easier to use for this particular problem.

Acknowledgements

This research project is partially sponsored by the National Science Foundation Grant No-CMS 9908016 and by the US Navy Office of Naval Research Advanced Electrical Power Systems Program.

References

Basaran, C., Zhao, Y., 2001. Mesh sensitivity and FEA for multilayered electronic packaging. Trans. ASME, J. Electron. Packag. 123 (3), 218–224.

Bert, C.W., 1984. A critical evaluation of new plate theories applied to laminated composites. Compos. Struct. 2, 329–347.

Bogy, D., 1968. Edge-bonded dissimilar orthogonal elastic wedges under normal and shear loadings. ASME, J. Appl. Mech. 35, 460–466.

Bogy, D.B., 1970. On the problem of edge-bonded elastic quarter-planes loaded at the boundary. Int. J. Solids Struct. 6, 1287–1313.

Chen, D., Cheng, S., Geerhardt, T.D., 1982. Thermal stresses in laminated beams. J. Therm. Stresses 5, 67–84.

Cho, K.N., Bert, C.W., Striz, A.G., 1987. New Theory for Bending of Bimodular Laminates. Engineering Science Preprint ESP24.87034, Univ. of Utah, Salt Lake City, Utah.

Hayashi, T., 1967. Analytical study of interlaminar shear stresses in a laminate composite plate. Trans. Jpn. Soc. Aeronaut. Space Sci. 10 (17), 43–48.

Hein, V.L., Erdogan, F., 1971. Stress singularities in a two-material wedge. Int. J. Fract. Mech. 7 (3), 317–330.

Lee, M., Jasiuk, I., 1991. Asymptotic expansions for the thermal stresses in bonded semi-infinite bimaterial strips. J. Electron. Packag. 113, 173–177.

Levinson, M., 1980. An accurate, simple theory of the statics and dynamics of elastic plates. Mech. Res. Commun. 7, 343–350.

Lo, K.H., Christensen, R.M., Wu, E.M., 1977a. A higher order theory of plate deformation—part I: homogeneous plates. ASME, J. Appl. Mech. 44, 663–668.

Lo, K.H., Christensen, R.M., Wu, E.M., 1977b. A higher order theory of plate deformation—part I: laminates plates. ASME, J. Appl. Mech. 44, 669–676.

Pagano, N.J., 1969. Exact solutions for composite laminates in cylindrical bending. J. Compos. Mater. 3, 398–411.

Pagano, N.J., 1974. On the calculation of interlaminar normal stress in a composite laminate. J. Compos. Mater. 8, 65–82.

Pagano, N.J., 1978. Stress fields in composite laminates. Int. J. Solids Struct. 14, 385–400.

Pipes, R.B., Pagano, N.J., 1970. Interlaminar stresses in composite laminates under uniform axial extension. J. Compos. Mater. 4, 538–548.

Rehfield, L.W., Valisetty, R.R., 1984. A simple refined theory for bending and stretching of homogeneous plates. AIAA J. 22 (1), 90–95.

Reissner, E., 1975. On transverse bending of plates including the effect of transverse shear deformation. Int. J. Solids Struct. 11, 569–573.

Shih, C.F., Asaro, R.J., 1988. Elasto-plastic analysis of cracks on bi-material interfaces: Part I—small scale yielding. ASME, J. Appl. Mech. 55, 299–316.

Shih, C.F., Asaro, R.J., 1989. Elasto-plastic analysis of cracks on bi-material interfaces: Part II—structure of a small-scale yielding fields. ASME, J. Appl. Mech. 56, 763–779.

Valisetty, R.R., 1983. Bending of Beams, Plates and Laminates: Refined Theories and Comparative Studies. Ph.D. thesis, Georgia Institute of Technology, Atlanta, March 1983.

Valisetty, R.R., Rehfield, L.W., 1983. A Theory for Stress Analysis of Composite Laminates. AIAA Paper 83-0833-CP, presented at the 24th AIAA/ASME/ASCE/AHS Structures, Structural Dynamics and Materials Conference, Lake Tahoe, NV, 2–4 May 1983.

Wang, A.S.D., Crossman, F.W., 1977. Some new results on edge effect in symmetric composite laminates. J. Compos. Mater. II, 92–106.

Wang, J.T.S., Dixon, J.N., 1978. Interlaminar stresses in symmetric composite laminates. J. Compos. Mater. 12, 390–402.

Washizu, K., 1968. Variational Methods in Elasticity and Plasticity. Pergamon, New York.

Williams, H.E., 1985. Asymptotic analysis of the thermal stresses in a two-layer composite with an adhesive layer. J. Therm. Stresses 8, 183–203.

Yin, W.L., 1991. Thermal stresses and free-edge effects in laminated beams a variational approach using stress functions. J. Electron. Packag. 113, 68–75.